Article

Consequences of *Lmna* exon 4 mutations in myoblast function

Déborah Gómez-Domínguez [1], Carolina Epifano [2], Fernando de Miguel [1,3], Albert García Castaño [4], Borja Vilaplana-Martí [1], Alberto Martín [1], Sandra Amarilla-Quintana [5], Anne T Bertrand [6], Gisèle Bonne [6], Javier Ramón-Azcón [4,7], Miguel A Rodríguez-Milla [1], Ignacio Pérez de Castro [1], *

[1] Instituto de Investigación de Enfermedades Raras; Instituto de Salud Carlos III; Ctra. Majadahonda-Pozuelo km2.2; E-28029 Madrid, Spain; d.gomez@isciii.es (D.G-D), ferdemiguelpe@gmail.com (F.M.), bvilaplana@isciii.es (B.V.M.), almmartin@isciii.es (A.M.), rmilla@isciii.es (M.R-M.), iperez@isciii.es (I.P.C.)

[2] Fundación Andrés Marcio, niños contra la laminopatía; C/Núñez de Balboa, 11, E-28001 Madrid, Spain; cepifano@hotmail.com (C.E.)

[3] Universidad Europea de Madrid; C/ Tajo, s/n, E-28670 Villaviciosa de Odón, Spain; ferdemiguelpe@gmail.com (F.M.)

[4] Institute for Bioengineering of Catalonia (IBEC), C/Baldiri Reixac, 10-12, E-08028 Barcelona, Spain; agarciac@ibecbarcelona.eu (A.G.C.), jramon@ibecbarcelona.eu (J.R.-A.)

[5] Fundación de Investigación HM Hospitales, Plaza del Conde Valle Suchil, 2, E-28015 Madrid, Spain; amarillaquintana@gmail.com (S.A-Q.)

[6] Sorbonne Université, INSERM UMRS 974, Center of Research in Myology, Institut de Myologie, Paris, France; a.bertrand@institut-myologie.org (A.B.), g.bonne@institut-myologie.org (G.B.)

[7] ICREA-Institució Catalana de Recerca i Estudis Avançats, 08010 Barcelona, Spain (J.R-A)

* Correspondence: iperez@isciii.es; Tel.: (+34 918223188)

Abstract: Laminopathies are causally associated with mutations on Lamin A gene (*LMNA*). To date, more than 400 mutations in *LMNA* have been reported in patients. These mutations are widely distributed throughout the entire gene and are associated with a wide range of phenotypes. Unfortunately, little is known about the mechanisms underlying the effect of the majority of these mutations. This is the case of more than 40 mutations that are located at exon 4. Using CRISPR/Cas9 technology, we have generated a collection of *Lmna* exon 4 mutants in mouse C2C12 myoblasts. These cell models include different types of exon 4 deletions and the presence of R249W mutation, one of the human variants associated with a severe type of laminopathy (*LMNA*-associated congenital muscular dystrophy). We have characterized these clones by measuring their nuclear circularity, myogenic differentiation capacity in 2D and 3D conditions, DNA damage, and p-ERK and p-AKT levels. Our results indicate that *Lmna* exon 4 mutants show abnormal nuclear morphology. In addition, levels and/or subcellular localization of different members of the lamin and LINC complex are altered in all these mutants. Whereas no significant differences were observed for ERK and AKT activities, the accumulation of DNA damage was associated to the *Lmna* p.R249W mutant myoblasts. Finally, significant myogenic differentiation defects were detected in the *Lmna* exon 4 mutants. These results have key implications in the development of future therapeutic strategies for the treatment of laminopathies.

Keywords: LMNA; laminopathy; CRISPR; nuclear envelope

1. Introduction

Laminopathies are a group of human rare diseases mainly associated with different mutations on Lamin A/C gene (*LMNA*). Laminopathies include at least 15 different diseases that are divided in four different categories depending on the affected tissues: striated muscle, adipose tissue, peripheral nerves or multiple tissues [1]. *LMNA* gene contains 12 exons and codes for two different proteins, Lamin A and C. Both are members of the intermediate filament group of proteins, which are characterized for the presence of a short N-terminal domain, a central domain composed of four α-helical domains that are separated by three linker regions and a globular C-terminal region. To date, almost 500 mutations in *LMNA* have been reported in patients (http://www.umd.be/LMNA/). These mutations are widely distributed throughout the entire gene. Moreover, there is no association between the gene location of these mutations and the wide range of phenotypes included in this group of rare diseases. Two main hypotheses have been postulated to explain the development and progression of laminopathies [2]. One of them assumes that *LMNA* mutations provoke structural and mechanical changes that are responsible for the development of the disease, while the other relies on functional abnormalities induced by changes in gene expression patterns and differentiation programs. Unfortunately, little is known about the exact mechanisms underlying the effects induced by the majority of the laminopathy-causing *LMNA* mutations.

No curative treatment is currently available for any type of laminopathy. A number of pre-clinical studies have explored the therapeutic potential of different compounds that modulate the mTOR/AKT pathway [3,4], the mitogen-activated protein kinase cascade [5,6] and the epigenetic regulator NAT10 [7], among others. Gene therapy approaches are being studied as well. In this regard, the most promising results have been obtained for Hutchinson-Gilford progeria syndrome (HGPS) by introducing frameshift mutations in the *LMNA* gene in a CRISPR/Cas9 dependent manner [8,9]. Besides these advances, we are still far from a cure for the majority of the laminopathies. More information is, therefore, needed about the molecular and cellular defects induced for each disease associated, *LMNA* mutation in order to get the therapeutic strategies that better fit each case.

Here we have explored whether mutations in *Lmna* exon 4 affect the biology and function of mouse myoblasts. This exon codes for a linker domain comprised between the two central α-helical domains of lamins A and C (**Figure S1**). Although up to 47 mutations in *LMNA* exon 4 have been reported with different disorders linked to this gene (http://www.umd.be/LMNA/), little is known about the cellular and molecular changes induced by them that are causally related with laminopathy development and progression. Since *LMNA* exons 3 and 5 are in frame, exon 4 skipping might be considered as a therapeutic strategy for all those laminopathies associated with *LMNA* exon 4 mutations. Although it has been reported that exon skipping could be successfully used for the treatment of diseases associated with *LMNA* mutations in exon 5 [10], the potential of this approach has not been tested yet for *LMNA* exon 4.

Using mouse C2C12 myoblasts and CRISPR/Cas9, we have generated a collection of *Lmna* exon 4 mutants that were classified as *Lmna*-null, *Lmna*-R249W or carriers of *Lmna*-exon4-in-frame-deletions. The study of these mutants allowed us to find critical information on the importance of *Lmna* exon 4 in myoblast biology, specifically in the integrity of the nucleus, the protein levels and sub-cellular location of nuclear envelope proteins and the capacity to differentiate to myogenic fibers. Given the fact that *LMNA* mutations are causally associated with several rare diseases, this work provides new and valuable information for a better understanding and future treatment of these diseases with no cure.

2. Materials and Methods

Cell lines and 3D model

For the majority of our experiments, we have used the C2C12 line (SIGMA 91031101), consisting of established myoblasts from the muscle of a tip on a C3H mouse line. C2C12 cells and selected clones with mutations in exon 4 of *Lmna* have been grown at a 37°C of temperature and 5% CO_2 conditions. The culture medium of myoblasts was based on DMEM (Dulbecco Modified Eagle

Medium) supplemented with 4.5 g/L glucose (Lonza), 10% bovine fetal serum (FBS) (Sigma) and 1% of penicillin/streptomycin (Lonza). Three human myoblast cell lines [11] have been used in this work. Two were controls isolated from a 25 and 88 year old, healthy individuals (C25CL48 and AB1079, respectively). A third myoblast cell line was isolate from a 3 year old, L-CMD patient who carried a *LMNA* p.R249W mutation. Human myoblasts were grown at a 37°C and 5% CO_2 conditions, in 1 volume of medium 199 (Invitrogen, 41150020) plus four volumes of DMEM (Invitrogen, 61965-026) with 20% fetal bovine serum (FBS), and supplemented with 25 µg/ml fetuin (Life Technologies, 10344026), 5 ng/ml hEGF, (Life Technologies, PHG0311), 0.5 ng/ml bFGF (Life Technologies, PHG0026), 5 µg/ml Insuline (Sigma, 91077C-1G) and 0.2 µg/ml Dexamethasone (Sigma D4902-100mg).

3D muscle models were fabricated by photo-molding technique as we described previously [12] (**Figure S2**). Gelatin-based polymer solution (see **Appendix A**) was mixed with a C2C12 cell suspension to reach the final cell density of $25x10^6$ cell/ml. Briefly, a 6µl drop of cell-laden polymer was placed on a functionalized coverslip (**Appendix A**), and a microstructured silicone (PDMS) stamp was pressed lightly on top filling the microchannels with the solution. The sizes of PDMS stamp consisting on grooves of 100 µm and 100 µm in height, and ridges of 100 µm. The hydrogel was photo-crosslinked using a UVP Crosslinker (Model CL-1000L, 365nm, 40W, from Analytik Jena US, Upland, USA) by the exposure of 30 s under UV light. After carefully removing the stamp, the micro-structured cell-laden hydrogels were incubated 1 day with culture medium. Due to high cell density in the hydrogel, growth medium was changed to differentiation medium, based in DMEM high glucose, supplemented with 2% horse serum (Thermofisher, #26050-088) and 1% penicillin/streptomycin, after 1 day to induce differentiation into myotubes.

Generation of clones with mutations in Lmna exon 4 using CRISPR/Cas9

All sgRNAs were designed to target exon 4 of the *LMNA* gene using the Breaking Cas Design tool (https://bioinfogp.cnb.csic.es/tools/breakingcas/) [13]. Three sgRNAs for the exon 4 *Lmna* (sg10: 5′-CCGGCTGGCAGATGCCCTGCAGG-3′, sg11: 5′-GCGGGCTCAGCATGAGGACCAGG-3′, and sg12: 5′-GGTCCACCTTGTCATATTCTTCC-3′) were cloned in the px459 vector (pSpCas9(BB)-2A-Puro, Addgene #62988). The C2C12 cells were transfected with the corresponding sgRNA (sg10, sg11 or sg12) cloned in the vector px459 and with the corresponding template (ssODN) in low (30pmol) or high (300pmol) doses and mutated only in the PAM (mut) or mutated in the PAM and in the Protospacer (mut2) (**Table 1**). In all the cases, we used Lipofectamine 3000 (Invitrogen, L3000015) and followed the manufactured directions. After 48 hours of transfection, puromycin (2 µg/ml) was added during 5 days. The selected cells were grown until a pool was obtained per condition. The clones were picked-up after seeding at low density of the pools. The pools and clones were expanded to allow the complete analysis. For the control samples, we follow the same process but using an empty px459 vector and no templates.

DNA sequencing and bioinformatic analysis

To identify mutations at *Lmna* exon 4, MiSeq DNA (Illumina, MS-102-2003) was carried out in the Genomic Unit of Instituto de Salud Carlos III. DNA was isolated from the different pools and clones. Next, the target region of the Cas9 nuclease was amplified with the DNA polymerase (NZYTech Nº Cat: MB354) adding the Illumina adapters by PCR: DeepSeq-Fw: TCGTCGGCAGCGTCAGATGTGTATAAGAGACAGAGGCGAGTGGATGCTGAG and DeepSeq-Rv: GTCTCGTGGGCTCGGAGATGTGTATAAGAGACAGGTCAATGCGGATTCGAGACT. This PCR product was used for a second PCR, where the specific indexes were added to every sample. Genomic reads in FASTQ format were analyzed using CRISPResso platform (http://crispresso.pinellolab.partners.org/). This software isolates the part of each read spanning the chosen region, highlights small insertions/deletions and outputs a count of each regional sequence. We then analyzed the percentage of the sequences showing regional differences in control and with the different sgRNA-Exon 4 of *LMNA*-transduced samples.

All the pools and clones, were also analyzed after Sanger sequencing of PCR products amplified using *Lmna* exon 4 specific primers (Sanger-mLmna_Ex4_Fw: 5'CCAGGCTAAGCGAGGGCTGC3' and Sanger-mLmna_Ex4_Rv: 5'CCTGAGGAAGGCATCCCTGG3'). Sanger sequences were analyzed using TIDE platform (Tracking of Indels by Decomposition; https://tide.deskgen.com/).

Table 1. Templates sequences.

Name	Sequence
ssODNmex4g10	GTGGAGATCGATAACGGGAAGCAGCGAGAGTTTGAGAGCCGGCTGGCAGATGCCCTG CAGGAGCTCTGGGCTCAGCATGAGGACCAGGTGGAACAGTATAAGAAGGAGCT
ssODNmex4g11	GAGTTTGAGAGCCGGCTGGCAGATGCCCTGCAGGAGCTCTGGGCTCAGCATGAGGAC CAGGTGGAACAGTATAAGAAGGAGCTAGAAAAGACATACTCCGCCAAGGTGCT
ssODNmex4g12	AGAGCCGGCTGGCAGATGCCCTGCAGGAGCTCTGGGCTCAGCATGAGGACCAGGTGG AACAGTATAAGAAGGAGCTAGAAAAGACATACTCCGCCAAGTGCTGGCCTCAT
ssODNmex4g10mut	GTGGAGATCGATAACGGGAAGCAGCGAGAGTTTGAGAGCCGGCTGGCAGATGCCCTG CAAGAGCTCTGGGCTCAGCATGAGGACCAGGTGGAACAGTATAAGAAGGAGCT
ssODNmex4g10mut2	GTGGAGATCGATAACGGGAAGCAGCGAGAGTTTGAGAGCCGTCTTGCCGACGCACTT CAAGAGCTCTGGGCTCAGCATGAGGACCAGGTGGAACAGTATAAGAAGGAGCT
ssODNmex4g11mut	GAGTTTGAGAGCCGGCTGGCAGATGCCCTGCAGGAGCTCTGGGCTCAGCATGAGGAC CAAGTGGAACAGTATAAGAAGGAGCTAGAAAAGACATACTCCGCCAAGGTGCT
ssODNmex4g11mut2	GAGTTTGAGAGCCGGCTGGCAGATGCCCTGCAGGAGCTCTGGGCACAACACGAAGAT CAAGTGGAACAGTATAAGAAGGAGCTAGAAAAGACATACTCCGCCAAGGTGCT
ssODNmex4g12mut	AGAGCCGGCTGGCAGATGCCCTGCAGGAGCTCTGGGCTCAGCATGAGGATCAGGTGG AACAGTATAAGAAGGAGCTAGAAAAGACATACTCCGCCAAGTGCTGGCCTCAT
ssODNmex4g12mut2	AGAGCCGGCTGGCAGATGCCCTGCAGGAGCTCTGGGCTCAGCATGAGGATCATGTTG AGCAATACAAAAAAGAGCTAGAAAAGACATACTCCGCCAAGTGCTGGCCTCAT

Western blot analysis

SDS–PAGE was performed using standard procedures. Briefly, cells were disrupted with RIPA buffer (150 mM NaCl, 1% NP-40, 0.5 % Sodium deoxycholate, 0.1 % SDS, 50 mM Tris-HCl pH 7.5 and protease and phosphatase inhibitors) for 10 min at 4°C. Samples were centrifuged at 14000 rpm at 4°C for 15 min. Protein concentration was quantified with the BCA system (Pierce, Cat. N. 23227) and Laemmli sample buffer was added. Western blot analyses were performed using standard procedures. These are the primary antibodies used in this work: anti-mouse Lamin A/C (E-1) (1:3000, Santa Cruz Biotechnology, sc-376248), anti-mouse α-tubulin (1:5000, Sigma-Aldrich, T9026), anti-mouse SUN1 BBmSun1 IgC2b X12.11 (1:50, donated by Dr. Colin Stewart), anti-rabbit SUN2 11905 (1:500, donated by Dr. Eric Schirmer), anti-rabbit p44/42 MAPK Erk1/2-137F5 (1:1000, Cell Signaling, #4695), anti-rabbit phospho-p44/42 MAPK Erk1/2 Thr202/Tyr204 D13.14.4E (1:1000, Cell Signaling #4370), anti-mouse Akt (pan) 40D4 (1:1000, Cell Signaling #2920), anti-rabbit phospho-Akt (Ser473) D9E (1:1000, Cell Signaling #4060), and anti-mouse phospho-histone H2A.X (Ser139) (1:500, Millipore, 05-636-I). HRP-labelled secondary antibodies (1:5000, GE Healthcare, NA931-1ML and NA934-1ML) were used and the detection was performed using the ECL western blotting system (Thermo Scientific, Pierce 32106).

Immunofluorescence microscopy

For 2D cultures, cells were plated onto coverslips and fixed with methanol 5 min at -20°C. Cells were incubated in blocking solution (0.1% BSA, 1% FBS, 1% horse serum in PBS, in the case of SUN2; 1% BSA, 2.5% goat serum, 2.5% donkey serum, 0.3% Triton X-100 in PBS, in the cases of lamin A/C, lamin B1 and emerin) during 30 min. Primary antibodies were diluted in the blocking solution. The following primary antibodies were used followed by incubation with fluorescence conjugated Alexa-Fluor secondary antibodies (1:500, Thermo Fisher Scientific, A32723, A32740 and A32731): anti-mouse lamin A/C (E-1) (1:500, Santa Cruz Biotechnology, sc-376248), anti-rabbit lamin B1 (1:100, Abcam, ab16048), anti-rabbit emerin (D3B9G) (1:100, Cell Signaling, #30853), anti-mouse SUN1

(BBmSun1 IgC2b X12.11) (1:50, donated by Dr. Colin Stewart) and anti-rabbit SUN2 11905 (1:200, donated by Dr. Eric Schirmer). Coverslips were mounted using Prolong® Gold with DAPI (Cell Signalling Technology, P36935). Images were captured using a Leica TCS SP5 confocal microscope and a 63X (HCX PL APO 63x 1.4 OIL).

For the 3D models, cells were fixed in a 10% formalin solution (Sigma-Aldrich). Then, hydrogels were washed with tris-buffered saline (TBS, BR0042, Canvax Biotech, Spain), permeabilized with 0.1% Triton X-100 (Sigma-Aldrich) in TBS for 15 m and blocked with a blocking buffer consisting of 0.3% Triton X-100 and 3% donkey serum (brand) in TBS for 2 h. Afterwards, samples were washed with TBS and incubated in a 1:200 anti-MYH7 (Thermofisher, PA5-69132) in blocking buffer (O/N, 4°C). Then, they were washed with TBS and incubated in 1:40 Rhodamin-Phalloidin (Thermofisher, R415) and 1:200 goat anti-rabbit A488 (Thermofisher, A11034) in blocking buffer (O/N, 4°C). After washing with TBS, nuclei were counterstained with DAPI (1µM, Thermofisher) for 15 min.

Nuclear morphology analyses

Cells (5,000 cells/well) were plated into cell culture black microplate 96-well with a glass bottom (Greiner Bio-one). After 24 h, the cells were fixed with methanol for 5 min at -20°C. The fixed cells were incubated with 2µL/mL Hoechst 33324 (Thermo Fisher Scientific, H3570) in PBS for 10 min at 37°C. Finally, nuclear morphology was evaluated by determining the circularity index using the Cytell Cell Imaging System (GE Healthcare Life Sciences). The circularity values are between 0 and 1 (a value of 1 corresponds to a perfect circle). For the nuclei morphology in the 3D muscle model, confocal microscopy images were analyzed using ImageJ software to obtain cell and nuclei descriptor data of orientation, aspect ratio and circularity.

Myogenic differentiation

Myoblast differentiation was induced by growth-medium exchange for the differentiation medium (DMEM with 2% horse serum (Thermofisher, 26050088) and 1% of penicillin/streptomycin (Lonza)). The cells were differentiated for 5 days. The cells ($1x10^5$ cells/m24well) were fixed with methanol for 5 min at -20°C, permeabilized with 0.05% Triton X-100 in PBS for 5 min at room temperature, and washed with PBS for 5 min. Then coverslips were blocked in blocking solution (15% FBS in PBS) for 30 min at room temperature. The cells were incubated with primary antibody against myosin heavy chain (MF20, dilution 1:50, DSHB Hybridoma) for 1 h at room temperature. The cells were washed with PBS three times for 5 min, incubated with secondary antibody anti-mouse Ig (1:500, Alexa Fluor 488, Thermo Fisher Scientific, A32723) for 45 min at room temperature and in the dark, and washed with PBS three times for 5 min. Coverslips were mounted using Prolong® Gold with DAPI (Cell Signalling Technology, P36935). Stained myotubes were visualized in a Leica DM4B microscope (Microsystems) using the 10X (N PLAN 10x/0.25 DRY) and 20X objectives (HC PL FLUOTAR 20x/0.55 DRY).

Quantification and statistical analysis

The levels of Lamin A/C, Lamin B1, SUN1 and SUN2 at the membrane were analyzed using ImageJ software (National Institutes of Health). In brief, individual lines of constant length were plotted perpendicular to the nucleus and used to evaluate peak fluorescence intensity using the PlotProfile feature from ImageJ. Random individual plot profiles of conditions were generated and quantify at the nuclei using the PlotProfile feature from ImageJ. In every set of experiments, all immunofluorescence images were taken under the same exposure conditions.

All the graphs and statistical analyses have been carried out with GraphPad 8.0 software. Error bars represent standard error of the mean. For bar graphs, the level of significance was determined by a two-tailed unpaired Student's *t*-test. Images were quantified using ImageJ (National Institutes of Health, Bethesda, Maryland).

3. Results

3.1. Generation of Lmna exon 4 mutations in C2C12 cells.

In order to produce *Lmna* exon 4 mutants by CRISPR/Cas9 technology, we designed three sgRNAs to target the Cas9 endonuclease to this *Lmna* region (**Figure 1a**). Following the scheme depicted in **Figure 1b** and detailed in Materials and Methods section, we produced a total of 18 pools and 210 clones in which CRISPR/Cas9 activity (insertions and deletions, Indels) was measured by TIDE and deep sequence analyses (**Table S1**). It is interesting to note that each sgRNA induced a different Indel pattern (**Figure S3**). One single nucleotide deletion was the most frequent event when using sg12 (present in 77% of the clones), while a wider spectrum of deletions and insertions was observed for sg10 and sg11 guides. Interestingly, deletions of 3 and 6 nucleotides, which produce in-frame deletions mutants, were mainly observed in sg11 transfected cells (they were detected in 20 and 35%, respectively, of the clones). Sequences with no Indels were detected in 3, 5 and 23% of the clones transfected with s10, sg11 and sg12 guides, respectively.

We also aimed at introducing the R249W mutation, one of the human variants associated with a severe type of laminopathy, *LMNA*-associated congenital muscular dystrophy. In all the transfections, we incorporated a donor template including the mutant nucleotide. Although five clones were positive for the R249W mutation, only one (g11H-D6, **Table 2**) was free of additional, nucleotide changes and, therefore, allowed the expression of this mutant form.

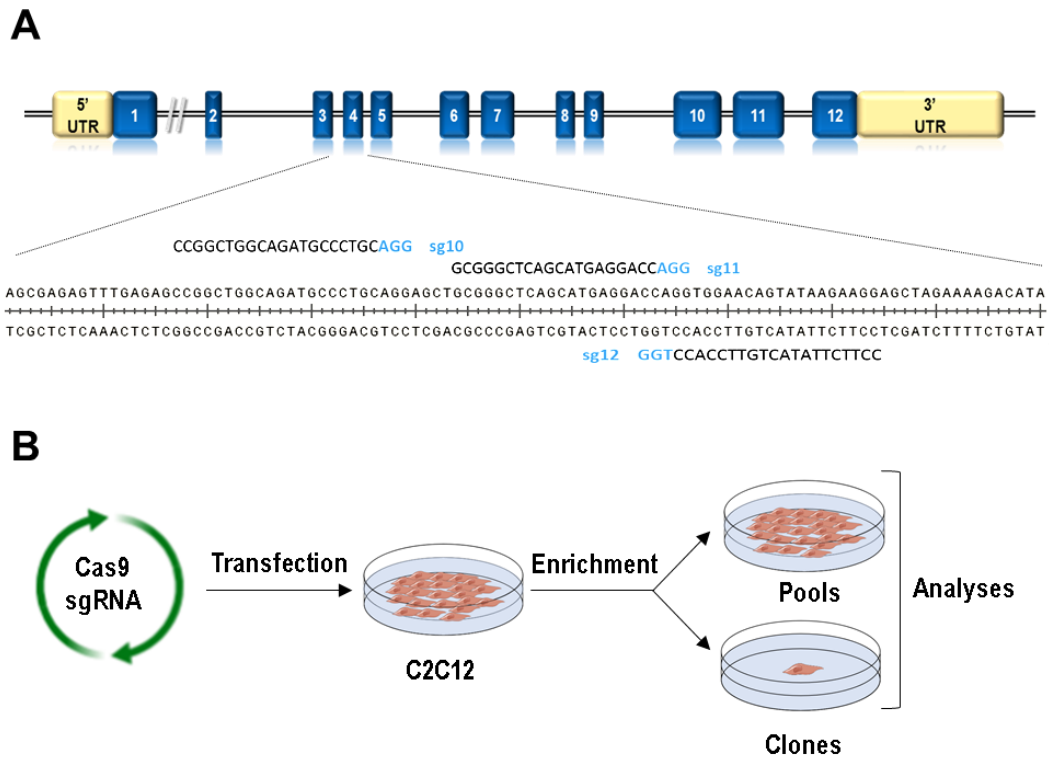

Figure 1. Generation of *Lmna* exon 4 mutations using CRISPR/Cas technology. **(A)** Scheme for exon 4 *Lmna* sgRNA localization. **(B)** Work-flow followed for the generation of C2C12 cells carrying mutations in *Lmna* exon 4.

One hundred and thirteen clones, named as "Null", only carried frameshift mutations that produced truncated proteins due to premature stop codons. Sixteen clones, classified as "Delta", were characterized by the only presence of triplete deletions compatible with the formation of Lamin A/C proteins with deletions of one, seven, fourteen, fifteen or fifty-seven aminoacids (**Figure S1**). Ten clones that were transfected with Cas9 expressing vectors with no sgRNAs, showed no mutations in

Preprints (www.preprints.org) | NOT PEER-REVIEWED | Posted: 15 April 2020 doi:10.20944/preprints202004.0232.v1

Peer-reviewed version available at Cells 2020, 9, 1286; doi:10.3390/cells9051286

Lmna exon 4 and were used and named as Controls. **Table 2** lists the Control, Null, Delta and R249W clones that were selected for a detailed study on the effects caused by the mutation in *Lmna* exon 4.

Table 2. Molecular properties of the selected clones.

ID	Type	CDS[1]	Protein (expected)
459-A6	Control	wt / wt	p.(666*) / p.(666*) (665 aa)
459-B4		wt / wt	p.(666*) / p.(666*) (665 aa)
g10L-A2	Null	c. 734_735del	p.(252*) (251 aa)
g11Hm-8		c. [757_758ins] [758_810del]	p.(263*) (262 aa)
g12Hm2-3		c. [767del] [811subsC>G]	p.(263*) (262 aa)
g12Lm2-3		c. [739_740ins] [740_761del] [766_767GT>AG]	p.(273*) (272 aa)
g12Lm2-5		c. [del767]/c. [del769]	p.(263*) (262 aa)/p.(263*) (262 aa)
g10L-A1	Delta1	c.734_736del (loss of 3 nt)	p.Leu245del (loss of 1 aa)
g11Hm2-1	Delta7-1	c.754_774del (loss of 21 nt)	p.His252_Gln258del (loss of 7 aa)
g11Hm2-10	Delta7-10	c.754_774del (loss of 21 nt)	p.His252_Gln258del (loss of 7 aa)
g10Hm-5	Delta14	c.707_748del (loss of 42 nt)	p.Glu236_Arg249del (loss of 14 aa)
g12Hm-6	Delta15	c.766_810del (loss of 45 nt)	p.Val256_Lys270del (loss of 15 aa)
g10H-A4	Delta57	c. [726_727ins] [727_1967del] /c. 640_810del	p.(252*) (251 aa)/p.Glu214_Lys270del (loss of 57 aa)
g11H-D6	R249W	c. [744_745subsGC>CT] [750subsT>G]	p.Arg249Tryp (665 aa)

[1] Obtained by deep sequencing

3.2. Lamin A/C *abnormal expression and subcellular localization in Lmna-exon-4 mutants.*

We first analyzed the protein levels and sub-cellular localization of Lamin A/C. As shown in **Figure 2a**, all the *Lmna*-exon-4 mutants were characterized by a significant reduction in the amount of both Lamin A and C proteins. This feature was accompanied by an abnormal subcellular localization of Lamin A/C in all Delta and R249W mutants (**Figure 2b**). Whereas Control and R249W myoblasts showed a predominant Lamin A/C signal in the nuclear periphery, Delta clones showed no differences in Lamin A/C intensity between perinuclear and nucleoplasmic regions. Moreover, in the different Delta clones we were able to detect a wide spectrum of abnormalities regarding Lamin A/C staining including honeycomb-like patterns, asymmetric distribution, capping and bright foci (**Figure S4**). Although Lamin A/C subcellular localization in R249W cells followed the same pattern found in Control myoblasts, a detailed analysis showed lower fluorescence intensity of Lamin A/C at the nuclear periphery and a discontinuous distribution with several gaps when compared with the Control clones (**Figure 2c**).

Our results indicate that a significant reduction and abnormal sub-cellular localization of Lamin A and C proteins in all the *Lmna* exon 4 mutants analyzed.

3.3. *Components of the nuclear lamin are abnormally distributed in Lmna-exon-4 mutant myoblasts.*

To investigate the consequences of the Lamin A/C mislocalization and low expression in *Lmna*-exon-4 mutants, we studied, using single confocal imaging, the sub-cellular localization of Lamin B1 and Emerin, two main inner nuclear membrane proteins. In Control clones, Lamin B1 accumulated at the nuclear periphery and was also detected, to a lesser extent, at the nucleoplasm. Lamin B1 distribution was slightly altered in *Lmna*-exon-4 mutants, which do not show a sharp contrast between the Lamin B1 signal detected in lamin area and nucleoplasm (**Figure 3a**). A significant effect was also expected for Emerin since the localization of this protein is dependent on Lamin A/C [14]. Indeed, Emerin sub-cellular distribution was affected in Null, Delta and R249W clones (**Figure3b**). In

Preprints (www.preprints.org) | NOT PEER-REVIEWED | Posted: 15 April 2020 doi:10.20944/preprints202004.0232.v1

Peer-reviewed version available at Cells 2020, 9, 1286; doi:10.3390/cells9051286

all the cases, Emerin extranuclear signal was compatible with the endoplasmic reticulum pattern previously reported for *Lmna* KO and mutant cells [15–17].

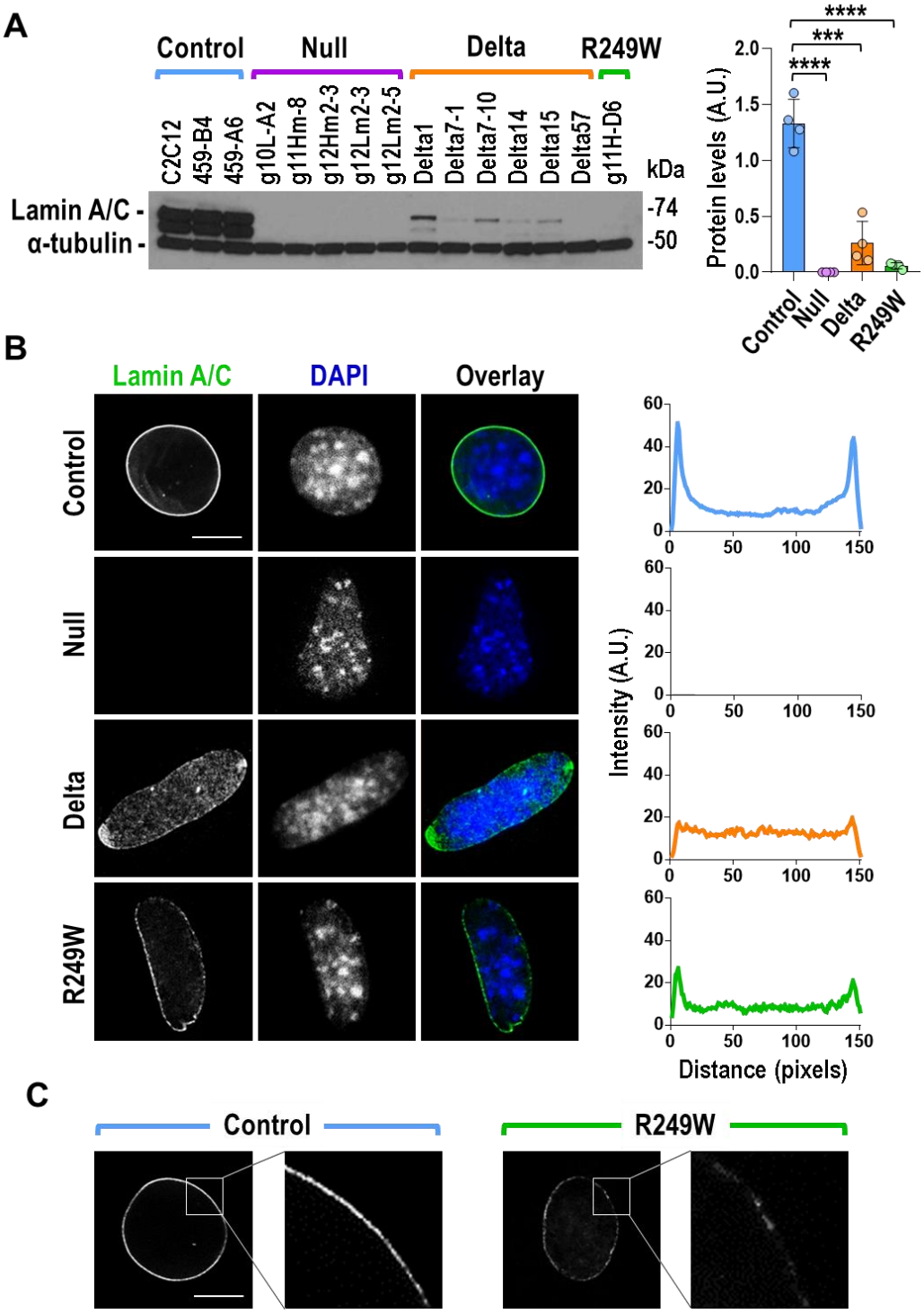

Figure 2. Lamin A and C levels and subcellular localization are altered in *Lmna* exon 4 mutants. **(A)** Quantification of Lamin A and C protein levels. Left pictures show one of the three independent biological replicates analyzed. Quantification of Lamin A/C signal in the three independent analyses, by mutant type, is shown on the right. Bars are mean±SEM,**** P<0.0001, *** P = 0.003, n=3. **(B)** Cells were immunostained for Lamin A/C (green) and nuclei was detected by DAPI staining (blue). Representative single confocal images from nuclei are shown for each *Lmna* group. Right plots show average Lamin A/C fluorescence intensity across nuclei by mutant type (Control: 3; clones; Null: 5 clones; Delta: 6 clones; R249W: 1 clone; n=5 nuclei per clone). **(C)** Immunofluorescence staining patterns of Lamin A/C in perinuclear area of representative control and R249W cells. Scale bar = 8μm.

Peer-reviewed version available at Cells 2020, 9, 1286; doi:10.3390/cells9051286

Therefore, *Lmna*-exon-4 mutations are associated with defects in the sub-cellular localization of the two main lamina components excluding Lamin A/C, Lamin B1 and Emerin.

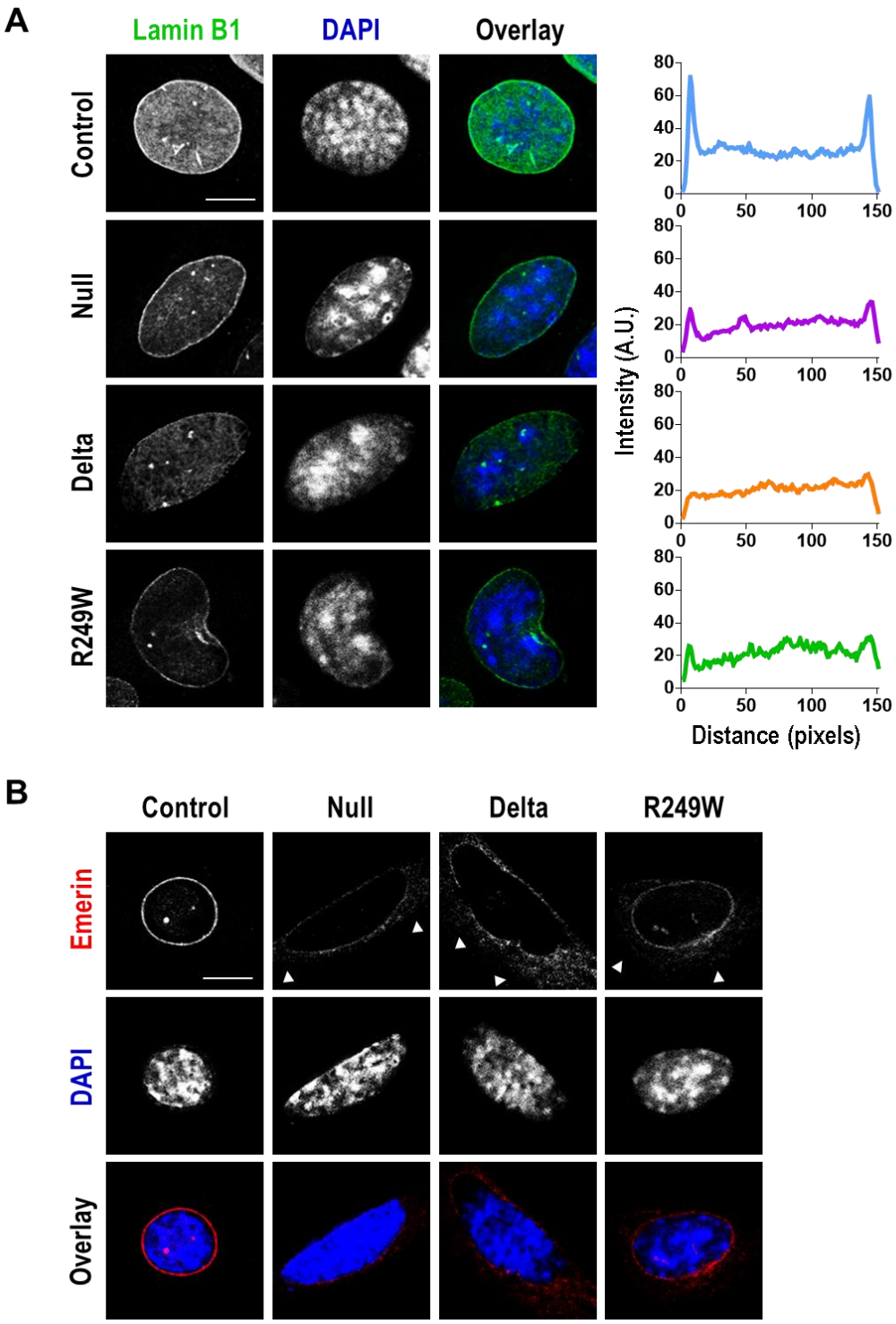

Figure 3. Components of the nuclear lamin are abnormally distributed in *Lmna*-exon-4 mutants. **(A)** Representative, single confocal images showing Lamin B1 detected by immunofluorescence. Plots show average fluorescence intensity across nuclei (3 Control, 5 Null, 6 Delta and 1 R249W clones; n=5 nuclei per clone). Peaks at both ends of the plot represent peripheral staining. **(B)** Representative, single confocal images of Emerin signal detected by immunofluorescence. Extra-nuclear signal is observed in null, delta and R249W mutants (arrows). Representative images from other clones are shown in **Figure S5** (Lamin B1) and **Figure S6** (Emerin).

Peer-reviewed version available at Cells 2020, 9, 1286; doi:10.3390/cells9051286

3.4. Nuclear morphology abnormalities are common for all the clones with mutations in Lmna exon 4.

The abnormalities described for all the *Lmna*-exon-4 mutants are compatible with a defective lamin that might affect the nuclear membrane integrity. To test this hypothesis we investigated the nuclear morphology of all the clones analyzed in this work. Whereas nuclei of Controls are circular or ovoid, mutant clones are characterized by irregular nuclei with multiple herniations and, more frequently, by elongated nuclei. To quantify these differences in terms of nuclear morphology, we calculated the circularity index of the nuclei of myoblasts asynchronously growing in 2D cultures. As expected, all the mutants showed a significant reduction in the circularity index of their nuclei (**Figure 4a**). To study nuclear morphology in a more physiologic condition, we encapsulated the myoblasts in a mimetic 3D architecture that recreated a native skeletal muscle (**Figure S2a**). Under this 3D cellular organization, all type of clones formed highly elongated and aligned fibers (**Figure S2b**). For both control and mutant clones, the circularity was reduced when compared to the values obtained in 2D experiments (**Figure 4b**). This effect is probably caused by the geometric constriction of the pattern and the compliant nature of the hydrogel used to create the 3D structure. Importantly, circularity was significantly reduced in mutant clones when they were compared to controls (**Figure 4b**).

These results demonstrate that mutations in *Lmna* exon 4 negatively affect nuclear morphology in myoblasts growing in both 3D and 2D conditions.

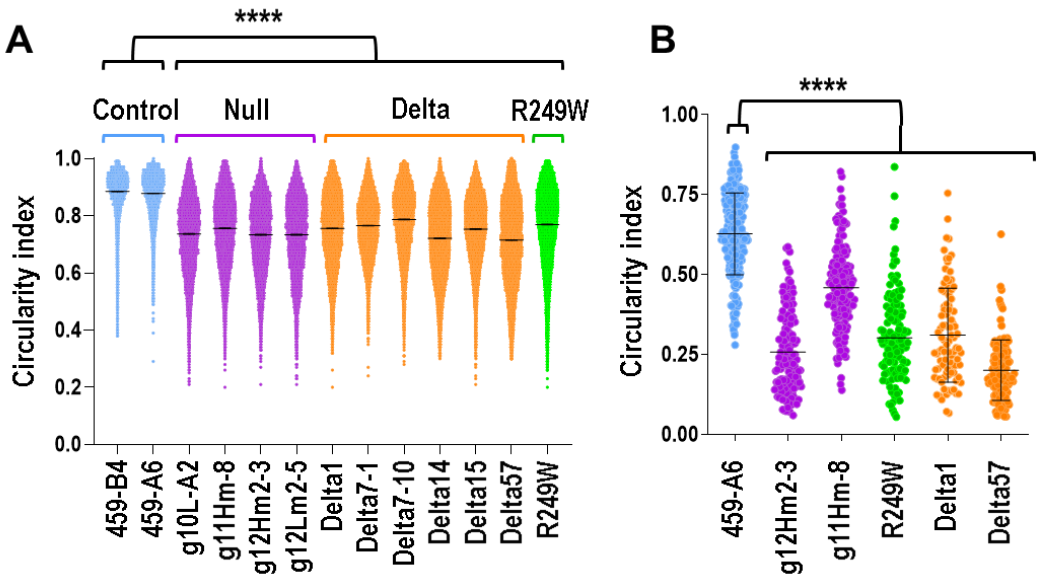

Figure 4. Nuclear morphology is altered in mouse myoblasts carrying *Lmna*-exon4 mutations. **(A)** Circularity index was calculated in nuclei from clones asynchronously growing in 2D cultures (**** P<0.0001; n>5000 nuclei per clone). **(B)** Plot shows the circularity index from clones encapsulated in a 3D pattern (**** P<0.0001). Blue, purple, green and orange colors indicate control, null, R249W and delta clones, respectively.

3.5. Abnormal myogenic differentiation is common to all myoblasts carrying Lmna exon 4 mutations.

LMNA mutations have been associated not only with structural abnormalities, such as the nuclear integrity defects described above, but also with functional deficiencies including differentiation capacity to myogenic fibers [18,19]. To test if this is also the case for the mutants generated in this work, we induced myogenic differentiation in all the myoblasts under study. In a first set of experiments, we studied the differentiation capacity of control and mutant clones growing in 2D conditions. As shown in **Figure 5a**, five days post induction of differentiation, Control myoblasts form myogenic fibers that are positive for myosin heavy chain (MHC). However, in Null, R249W and the majority of the Delta clones, we were not able to detect neither myogenic fibers nor

Peer-reviewed version available at Cells 2020, 9, 1286; doi:10.3390/cells9051286

MHC expression. Interestingly, Delta57 clone, which is missing the whole *Lmna* exon 4, showed a moderate formation of fibers and MHC expression.

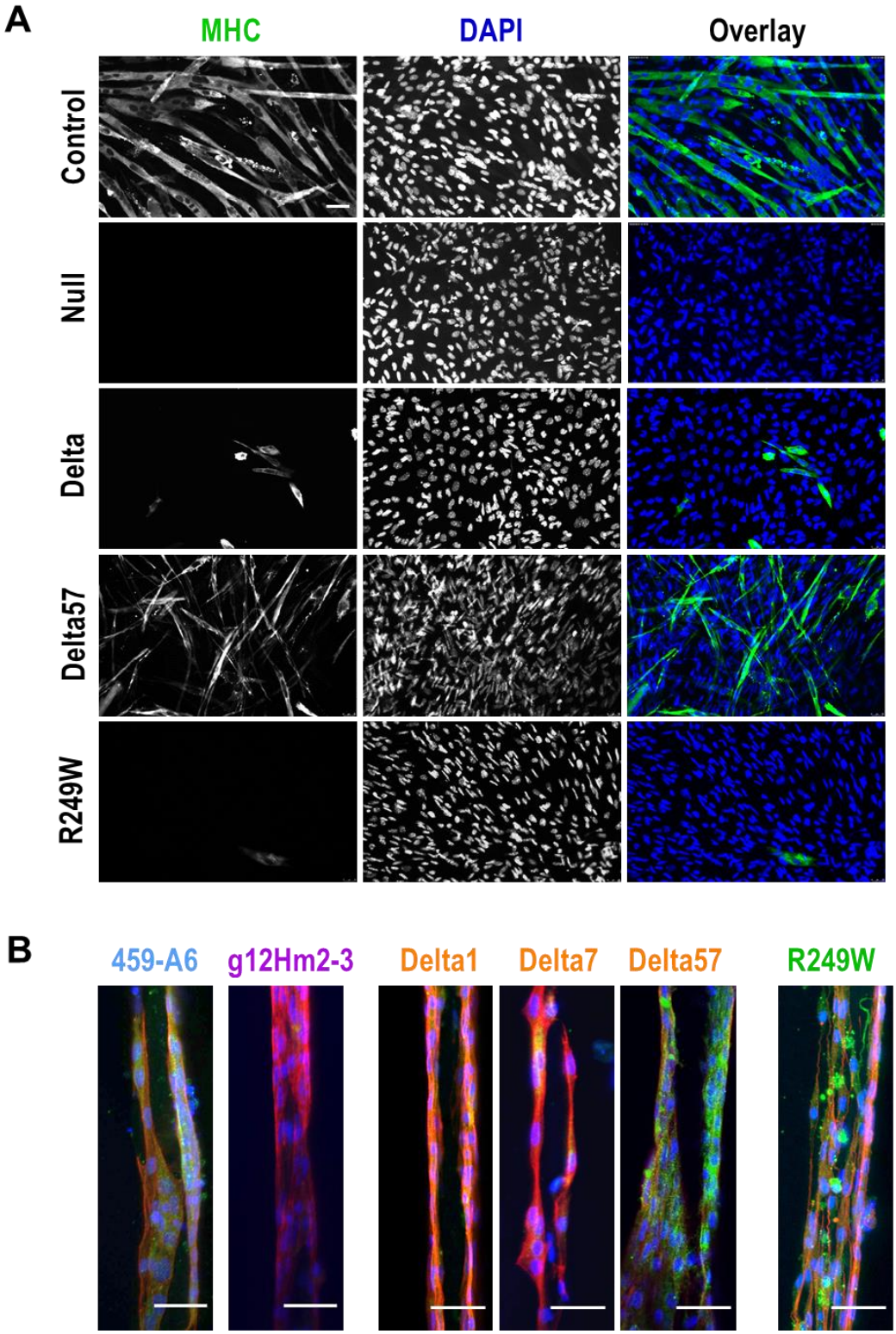

Figure 5. Myogenic differentiation is impaired in mouse myoblasts with mutations in *Lmna* exon 4. **(A)** Myoblasts growing in 2D conditions were induced to differentiate to myogenic fiber as described in Materials and Methods. Representative pictures show myosin heavy chain (MHC, green) and nuclei (DAPI, blue). Scale bar = 60 μm. **(B)** Myogenic fiber formation is also affected in 3D models. Representative pictures show, at 7 days post-differentiation, myosin heavy chain 7 (green), nuclei (blue) and phalloidin staining (red). Scale bar = 50 μm.

Similar results were obtained from myoblasts growing in 3D structures (**Figure 5b**). In this case, MHC was only detected in Control clones as well as in Delta57 and R249W mutants. Importantly, although R249W cells were positive for MHC, they showed an abnormal distribution of this protein that could indicate the formation of abnormal myogenic fibers.

Our results indicate that *Lmna* exon 4 mutations significantly affect the capacity of C2C12 cells to differentiate to myogenic fibers.

3.6. Expression of Lmna exon 4 mutants is associated with abnormal subcellular localization of SUN1 and SUN2.

In an effort to understand the mechanisms underlying the nuclear morphology and myogenic differentiation defects that characterize the *Lmna*-exon-4 mutants, we studied the status of SUN1 and SUN2. These proteins, together with Lamin A/C, Emerin and Nesprins among others, constitute the LINC complex, a molecular link that connects the nucleus to the cyto-skeleton and have been associated with muscular dystrophies [20]. The total protein level of SUN1 and SUN2 was not altered in any of the mutant types, either Null, Delta or R249W (**Figure 6a**). However, their subcellular distribution was significantly affected in all the mutants when compared with Controls (**Figure 6b**). Whereas SUN1 and SUN2 accumulated in the nuclear envelope of Control myoblasts, they were barely detected in the same region of *Lmna* exon 4 mutants.

These results together with the ones obtained for the localization of Emerin and Lamin proteins, indicate that the defects induced at the nuclear envelope by the *Lmna* exon 4 mutations, significantly impact on the subcellular localization of LINC complex components.

3.7. MAPK signaling is not altered in Lmna exon 4 mutant myoblasts.

Thanks to the analysis of the $Lmna^{H222P}$ mouse model it has been discovered a connection between *LMNA* mutations and signaling pathways [21]. Specifically, enhanced phosphorylation of ERK1/2 and AKT has been reported in the heart of $Lmna^{H222P}$ mice [5,22]. Therefore, we decided to study the status of these key signaling molecules in *Lmna*-exon-4 mutants. Although the activation of ERK1/2, estimated by the quantification of phosphorylated-ERK1/2, is very heterogeneous, no significant differences were observed when Control, Null, Delta and R249W clones were compared (**Figure 7a**). Likewise, there were not significant differences in AKT activation (**Figure 7b**).

Therefore, the *Lmna* exon 4 mutations studied here are not characterized for significant changes in the activation of the signaling proteins ERK1/2 and AKT.

3.8. High levels of DNA damage are associated with R249W mutation.

We also wanted to study the effect of *Lmna*-exon-4 mutations at the DNA level, since progeroid and striated muscle laminopathies have been associated with high levels of DNA damage [23–26]. Quantification of DNA damage by staining for γH2AX revealed elevated levels of DNA damage in the R249W clone while no signal was detected in the rest of mutants (Null and Delta) or Controls (**Figure 8a**). To further analyze the connection between the R249W mutation and DNA damage, we also explored it in human myoblasts carrying a *LMNA* p.R249W mutation causing L-CMD. Interestingly, the R249W mutant showed a significant increase in γH2AX levels when compared with the controls (**Figure 8b**).

These results indicate that high levels of DNA damage are a specific feature of *LMNA* p.R249W myoblasts.

Preprints (www.preprints.org) | NOT PEER-REVIEWED | Posted: 15 April 2020 doi:10.20944/preprints202004.0232.v1

Peer-reviewed version available at Cells 2020, 9, 1286; doi:10.3390/cells9051286

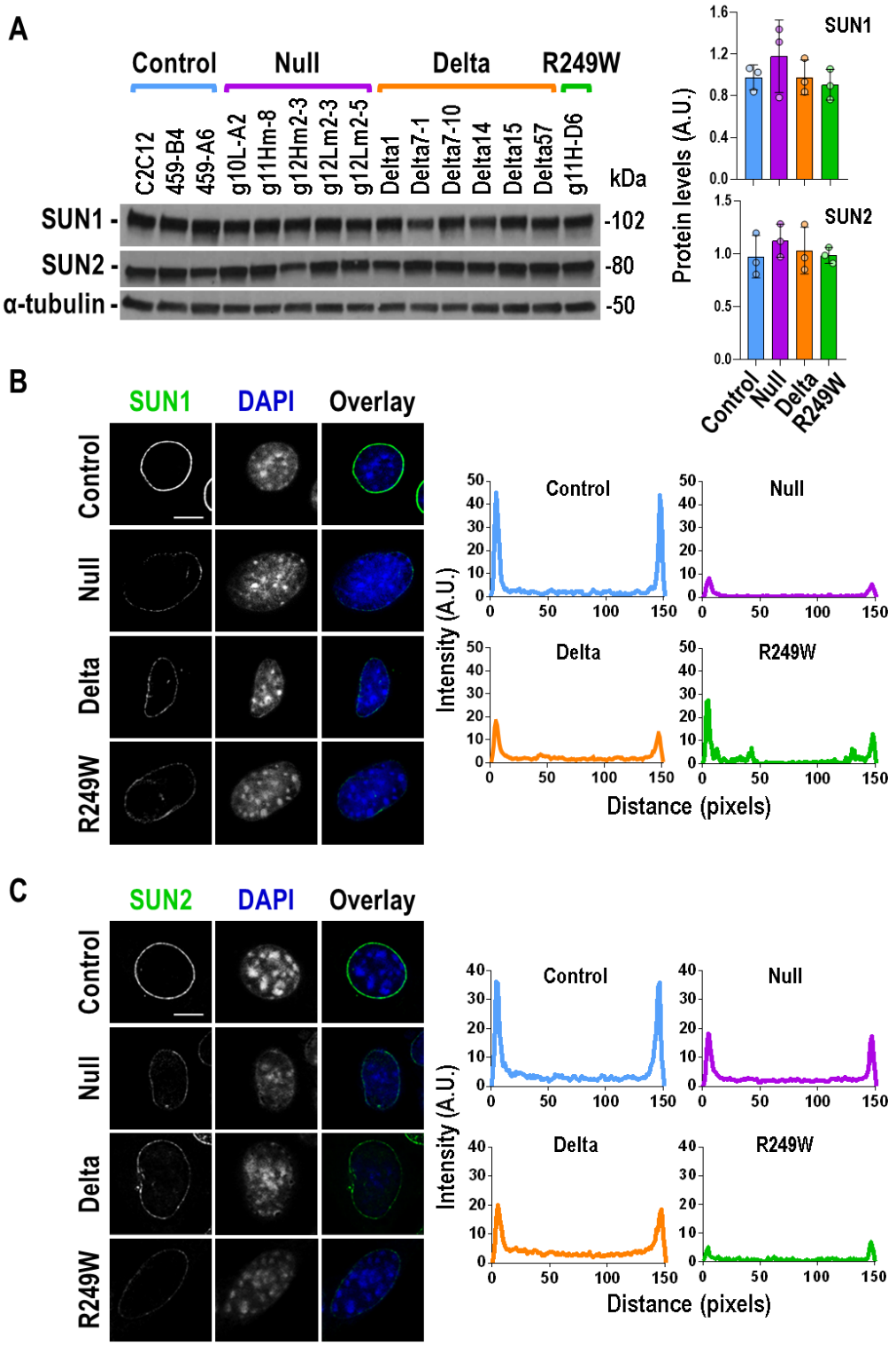

Figure 6. SUN1 and SUN2 protein levels and sub-cellular localization in *Lmna* exon 4 mutants. **(A)** Total amount of SUN1 and SUN2 proteins was determined by western blot. One of the three biological replicates is shown. Quantification, by mutant type, of SUN1 and SUN2 signals for the three independent analyses, is shown in right graphs. Bars are mean ± SEM, n=3. No significant differences were detected when mutants were compared with Controls. Representative, single, confocal, images of SUN1 **(B)** and SUN2 **(C)** detected by immunostaining are shown. A decreased nuclear envelope signal is observed in Null, Delta and R249W mutants. Scale bar = 8μm. Representative images for SUN1 and SUN2 in all the clones are shown in **Figure S7** and **Figure S8**, respectively.

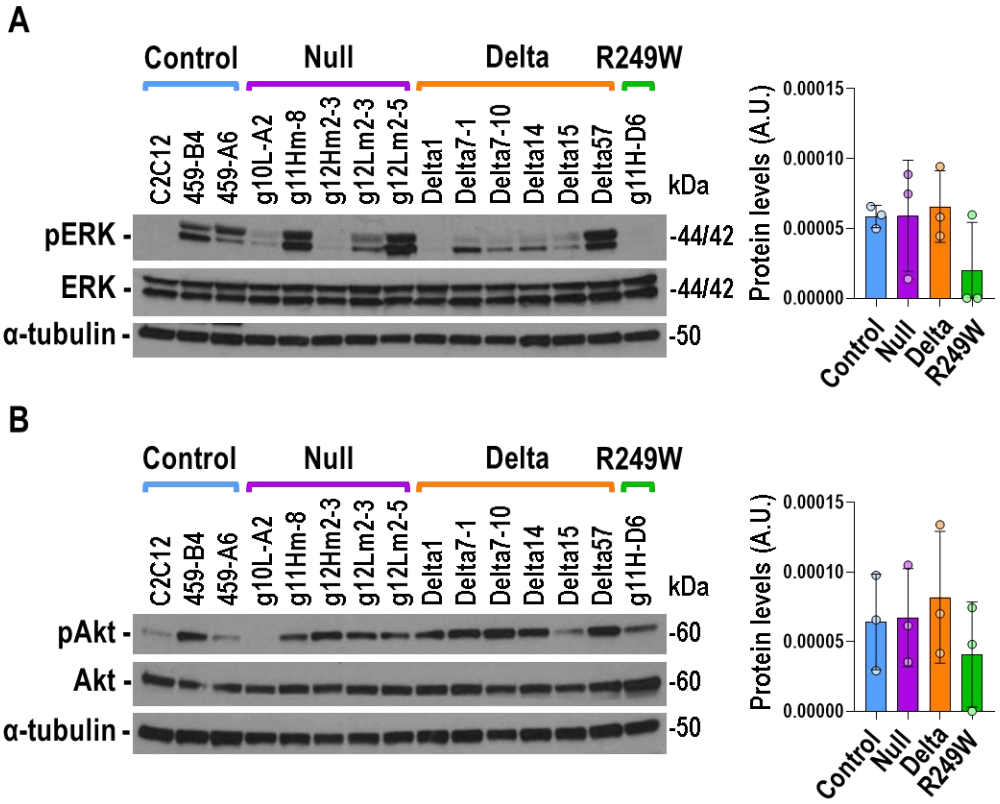

Figure 7. No differences in ERK1/2 and AKT activation are detected in *Lmna* exon 4 mutant myoblasts. **(A)** Representative immunoblot for the detection of phosphorylated (pERK) and total (ERK) ERK1/2 in *Lmna* exon 4 mutants. **(B)** Representative immunoblot for the detection of phosphorylated (pAKT) and total (AKT) AKT. Detection of α-tubulin was used in all the cases as loading control. Data in bar graphs are mean ± SEM of all the clones of each type, n=3. No significant differences were detected when mutants were compared with Controls.

4. Discussion

Comparison of Lmna exon 4 mutants generated in this study with previously reported LMNA mutants.

In this study, using CRISPR/Cas9 technology, we have analyzed a collection of *Lmna* exon 4 mutants in C2C12 mouse myoblasts. Three different types of mutants have been generated: Null mutants, due to frame shift mutations, Delta mutants, caused by in-frame deletions and a R249W mutant. Upon studying a number of molecular, cellular and functional features, we can conclude that the subcellular localization of key members of the LINC complex and nuclear envelope, including Lamin A/C, Lamin B1, Emerin, SUN1 and SUN2, as well as the nuclear membrane integrity and myogenic differentiation capacity are negatively affected.

The comparison of the features of the *Lmna* mutants described here with those previously reported by others results in coincidences and differences. For instance, the Emerin extranuclear localization, compatible with endoplasmic reticulum, detected in Null, Delta and R249W clones is similar to the previously reported for *Lmna* null, $Lmna^{L530P/L530P}$, $Lmna^{dK32}$ and $Lmna^{N195K}$ mouse myoblasts, and *LMNA* p.Y259X patient cells [15–17,27,28]. Contradictory results have been described for Lamin B1 localization. It has been reported that the loss of A-type lamins allows the assembly of B-type lamins [15]. However, more recently, LMNB1 localization defects have been shown in iPS cells carrying *LMNA* mutations [29], which is in line with the results we have obtained in the present work. On the other hand, the *Lmna*-Null, Delta and R249W analyzed in this work showed a nuclear, although low intensity, signal for SUN1 at the nuclear envelope. These results differ from the ones obtained in *Lmna null* or $Lmna^{L530P/L530P}$ mouse fibroblasts where a extranuclear signal or loss of nuclear

envelope signal has been reported [17,30]. We have no clear explanation for this apparent contradiction and, therefore, further studies are needed to solve it.

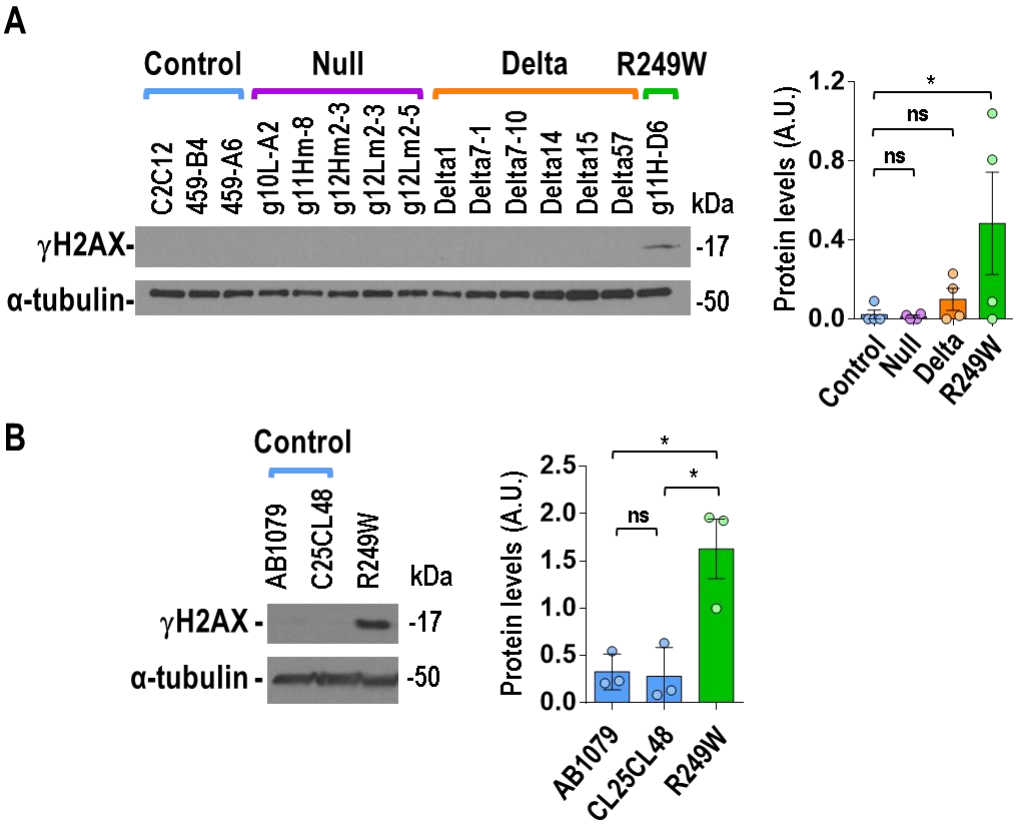

Figure 8. High levels of DNA damage are specifically associated with *LMNA* R249W mutation. **(A)** Representative immunoblot showing γ-H2AX levels in *Lmna* exon 4 mutants. **(B)** Immunoblot shows -H2AX levels in human myoblasts from 2 controls and 1 patient carrying the p.R249W mutation. Detection of -tubulin was used in all the cases as loading control. Data in bar graphs are mean ± SEM, n=3.

LMNA p.H222P, one of the most studied *LMNA* mutations, is also located in exon 4. However, some of its features differ from the data obtained with the exon 4 mutants analyzed here. For instance, the alterations of MAPK and AKT signaling pathways described in $Lmna^{H222P\text{-}H222P}$ model [5,22], are not detected in the *Lmna* exon 4 mutants analyzed in this work. This could indicate that the *Lmna*-p.H222P mutation alter specific signaling pathways while other *Lmna* exon 4 mutants do not. Another possible explanation, would be the fact that the majority of the studies for *Lmna* p.H222P have been carried out using cardiomyocytes from a $Lmna^{H222P}$ knockin mouse model, while the cells used in the present study are mouse myoblasts. The detailed characterization of the same cell type from a mouse $Lmna^{R249W}$ model (currently under study) will help us to discern the correct explanation of these differences.

Mechanistic and functional defects associated with Lmna exon 4 mutations

Myogenic differentiation is the most important function of myoblasts. It has been previously shown that the expression of lamin mutations associated with different laminopathies inhibits the *in vitro* differentiation of C2C12 myoblasts [18,19]. Abnormal myoblast differentiation has also been reported in $Lmna^{dK32}$ cells [28]. Moreover, *Lmna* null satellite cells are characterized by a defective myogenic differentiation [31]. The same defects are observed for the majority of the Null, Delta and

Peer-reviewed version available at Cells 2020, 9, 1286; doi:10.3390/cells9051286

R249W mutants analyzed in this work, which confirms the fact that mutations and/or downregulation of Lamin A/C are associated with an impairment in myogenic differentiation that might explain a significant part of the pathological phenotype of laminopathies. Regarding the mechanisms underlying this defective differentiation, an abnormal function of the LINC complex might be among the best possible candidates. The abnormal subcellular localization observed for many of the LINC complex components (Emerin, Lamin A/C, Lamin B1 and SUN1-SUN2) in *Lmna* exon 4 mutant myoblasts could be the cause of the defects detected in nuclear membrane integrity and myogenic differentiation. Interestingly, the LINC complex, a molecular link between the nucleo- and the cyto-skeleton, has been associated with muscular dystrophies [20]. However, additional studies are needed to confirm the causal relationship between *Lmna* exon 4 mutations and LINC complex in laminopathies.

DNA damage: a feature specific for the R249W mutation?

The nuclear lamina is a critical structure for the stability and proper nuclear distribution of DNA [32]. A weak nuclear envelope affects DNA integrity inducing the accumulation of DNA damage, a feature linked to *LMNA*-associated diseases [26,33–35]. The majority of the mouse myoblasts studied in this work did not show elevated levels of DNA damage, which is consistent with the fact that we have explored this property only in undifferentiated myoblasts and increased levels DNA damage are mainly observed in differentiated cells and tissues of HGPS and *LMNA*-related muscular dystrophies [26,34]. Surprisingly, even in this undifferentiated myoblast state, the *Lmna*-R249W mutant under study showed significantly elevated levels of DNA damage. The fact that this feature is also observed in human *LMNA* p.R249W myoblasts (**Figure 8**) and in muscle biopsies from a 1 year-old patient carrying a *LMNA* p.R249W mutation [26] points out to a specific association with DNA integrity and/or repair mechanisms. Further studies will help to validate this connection and explore therapeutic opportunities related with DNA damage and repair.

CRISPR/Cas9 activity and Gene therapy implications

The Delta and R249W clones analyzed in this work show a significant reduction in the levels of Lamin A/C (**Figure 1**). This is probably due to the CRISPR-mediated deletion of one or more *Lmna* alleles (C2C12 cells used in this work are hypertriploid) since mRNA expression is significantly reduced in all of them (data not shown). Therefore, the phenotypes observed in the *Lmna* exon 4 mutants could be due, not only to the mutations generated in *Lmna*, but also to a defective expression of lamin proteins. It is important to note that *Lmna* haploinsufficiency is associated with dilated cardiomyopathy [36]. All these evidences have important implications for the therapeutic potential that CRISPR technology could have for the treatment of laminopathies.

One of the most interesting results we have obtained in this work is the high percentage of Delta clones isolated upon CRISPR/Cas9 activity on *Lmna* exon 4 (**FigureS1**). This indicates that this type of in-frame mutations might have some selective advantage over the rest of *Indels* generated by CRISPR/Cas9 activity. Moreover, one of these clones, Delta57, is characterized by the expression of a *Lmna* exon 4 null gene. Interestingly, although Delta57 shows nuclear morphology and LINC complex abnormalities, it does retain some myogenic differentiation capacity. This could indicate that an exon 4 skipping strategy for the elimination of mutations located in this exon could be compatible with a partially functional myoblast. As far as we know, in *LMNA*-associated disease, successful exon skipping has only been shown for exon 5 in human cells [10]. The potential of this therapeutic strategy needs further experimentation in appropriate *in vivo* models.

In conclusion, with this work we have characterized in detail the consequences associated with mutations in *Lmna* exon 4 in myoblasts. This new knowledge has opened the possibility to explore new therapeutic approaches based on the DNA damage specifically induced by the *Lmna*-R249W mutation and the use of exon skipping strategies for the elimination of *Lmna* exon 4 mutations.

Supplementary Materials: The following are available online at www.mdpi.com/xxx/s1.

- Table S1: Sequencing information of *Lmna* exon 4 mutant clones and pools.
- Figure S1: Scheme of the *Lmna* gene and protein structure and the mutants generated in this work.
- Figure S2: Generation of 3D skeletal muscle models.
- Figure S3: Deletions/insertions detected in C2C12 pools and clones.
- Figure S4: Lamin A-C subcellular localization and expression in Delta mutants.
- Figure S5: Lamin B1 subcellular localization in *Lmna* exon 4 mutants
- Figure S6: Emerin subcellular localization in *Lmna* exon 4 mutants.
- Figure S7: SUN1 sub-cellular localization in Lmna exon 4 mutants
- Figure S8: SUN2 sub-cellular localization in Lmna exon 4 mutants

Author Contributions: Conceptualization, I.P.C.; Methodology, D.G-D., C.E., F.M., A.G.C, J.R-A., I.P.C.; Investigation, D.G-D., C.E., F.M., A.G.C, B.V-M., A.M., S.A-Q., M.R-M.; Resources, A.T., G.B.; Writing—original draft preparation, D.G-D., C.E., I.P.C.; Writing—review and editing, D.G-D., C.E., F.M., A.G.C, B.V-M., A.M., S.A-Q., A.B., G.B., J.R-A, M.R-M, I.P.C.; Supervision, I.P.C..; Project administration, I.P.C.; Funding acquisition, F.M., I.P.C. All authors have read and agreed to the published version of the manuscript.

Funding: This research was funded by *Ministerio de Ciencia e Innovación* (Acción estratégica en Salud intramural PI16III/00017-TPY1348/16) and by *Fundación Andrés Marcio, niños contra la laminopatía* (TPY-259/19). F.M. was funded by a *Miguel Servet II* contract from ISCIII.

Acknowledgments: We thank all the members of the Human Genetics Area of the Instituto de Investigación de Enfermedades Raras (IIER) for their continuous support and help. We are deeply grateful to Dr. Beatriz Martínez (IIER) for the logistic and scientific support at the beginning of the project. The authors thank Dr. Oscar Zaragoza for confocal microscopy assistance. We are very grateful to Dr. Eric Schirme and Dr. Colin Stewart for kindly providing SUN2 and SUN1 antibodies.

Conflicts of Interest: The authors declare no conflict of interest. The funders had no role in the design of the study; in the collection, analyses, or interpretation of data; in the writing of the manuscript, or in the decision to publish the results.

Appendix A

Synthesis of prepolymer precursors

Gelatin methacryloyl (GelMA) was synthesized with a 40% degree of methacrylation as previously described (García-Lizarribar, Fernández-Garibay *et al*. 2018). The material was then dialyzed in Milli Q water with 6-8 kDa MWCO membranes (Spectrumlabs, 08-700-142) for 4 days. Sodium carboxymethylcellulose (CMC) (Sigma Aldrich, 419273) was methacrylated at a maximum degree of methacrylation as previously described (García-Lizarribar, Fernández-Garibay *et al*. 2018). The methacrylation reaction was performed by mixing a solution of 1% (w/v) of the polymer in 50 mM MES buffer at pH 6.5 with 20 mM EDC, 10 mM N-hydroxysuccinimide (Sigma Aldrich, 130672) and 10 mM 2 aminoethylmethacrylate (Sigma Aldrich, 479659). The reaction was stopped after 24 h with the addition of acetone (Panreac, 161007) and filtered using a vacuum flask. The precipitate was dissolved in PBS 10 mM and dialyzed in Milli Q water with 3.5 kDa MWCO membranes (Thermofisher, 68035). Finally, the solutions of methacrylated polymers (GelMA and CMCMA) were lyophilized and stored at -20°C.

Preparation of prepolymer solutions

A mixture of the prepolymer precursors (GelMA and CMCMA) was diluted in growth medium, containing the photoinitiator lithium Phenyl (2,4,6-trimethylbenzoyl) phosphinate (LAP) (TCI EUROPE N.V, L0290), at 65°C for 3 h to obtain a homogeneous solution. The concentrations of GelMA, CMCMA and LAP were fixed to obtain final concentrations of 5%, 1% and 0.1% (w/v), respectively

References

1. Worman, H.J. Nuclear lamins and laminopathies. *J. Pathol.* **2012**, *226*, 316–325.
2. Gruenbaum, Y.; Foisner, R. Lamins: Nuclear Intermediate Filament Proteins with Fundamental Functions in Nuclear Mechanics and Genome Regulation. *Annu. Rev. Biochem.* **2015**, *84*, 131–164.
3. Cenni, V.; Capanni, C.; Mattioli, E.; Columbaro, M.; Wehnert, M.; Ortolani, M.; Fini, M.; Novelli, G.; Bertacchini, J.; Maraldi, N.M.; et al. Rapamycin treatment of Mandibuloacral dysplasia cells rescues localization of chromatin-associated proteins and cell cycle dynamics. *Aging (Albany. NY).* **2014**, *6*, 755–70.
4. Pellegrini, C.; Columbaro, M.; Capanni, C.; D'Apice, M.R.; Cavallo, C.; Murdocca, M.; Lattanzi, G.; Squarzoni, S. All-trans retinoic acid and rapamycin normalize Hutchinson Gilford progeria fibroblast phenotype. *Oncotarget* **2015**, *6*, 29914–28.
5. Muchir, A.; Pavlidis, P.; Decostre, V.; Herron, A.J.; Arimura, T.; Bonne, G.; Worman, H.J. Activation of MAPK pathways links LMNA mutations to cardiomyopathy in Emery-Dreifuss muscular dystrophy. *J. Clin. Invest.* **2007**, *117*, 1282–1293.
6. Muchir, A.; Wu, W.; Choi, J.C.; Iwata, S.; Morrow, J.; Homma, S.; Worman, H.J. Abnormal p38 mitogen-activated protein kinase signaling in dilated cardiomyopathy caused by lamin A/C gene mutation. *Hum. Mol. Genet.* **2012**, *21*, 4325–4333.
7. Larrieu, D.; Britton, S.; Demir, M.; Rodriguez, R.; Jackson, S.P. Chemical Inhibition of NAT10 Corrects Defects of Laminopathic Cells. *Science (80-.).* **2014**, *344*, 527–532.
8. Beyret, E.; Liao, H.-K.; Yamamoto, M.; Hernandez-Benitez, R.; Fu, Y.; Erikson, G.; Reddy, P.; Izpisua Belmonte, J.C. Single-dose CRISPR–Cas9 therapy extends lifespan of mice with Hutchinson–Gilford progeria syndrome. *Nat. Med.* **2019**, *25*, 419–422.
9. Santiago-Fernández, O.; Osorio, F.G.; Quesada, V.; Rodríguez, F.; Basso, S.; Maeso, D.; Rolas, L.; Barkaway, A.; Nourshargh, S.; Folgueras, A.R.; et al. Development of a CRISPR/Cas9-based therapy for Hutchinson–Gilford progeria syndrome. *Nat. Med.* **2019**, *25*, 423–426.
10. Scharner, J.; Figeac, N.; Ellis, J.A.; Zammit, P.S. Ameliorating pathogenesis by removing an exon containing a missense mutation: a potential exon-skipping therapy for laminopathies. *Gene Ther.* **2015**, *22*, 503–515.
11. Bertrand, A.T.; Ziaei, S.; Ehret, C.; Duchemin, H.; Mamchaoui, K.; Bigot, A.; Mayer, M.; Quijano-Roy, S.; Desguerre, I.; Lainé, J.; et al. Cellular microenvironments reveal defective mechanosensing responses and elevated YAP signaling in LMNA-mutated muscle precursors. *J. Cell Sci.* **2014**, *127*, 2873–84.
12. Ortega, M.A.; Fernández-Garibay, X.; Castaño, A.G.; De Chiara, F.; Hernández-Albors, A.; Balaguer-Trias, J.; Ramón-Azcón, J. Muscle-on-a-chip with an on-site multiplexed biosensing system for in situ monitoring of secreted IL-6 and TNF-α. *Lab Chip* **2019**, *19*, 2568–2580.
13. Oliveros, J.C.; Franch, M.; Tabas-Madrid, D.; San-León, D.; Montoliu, L.; Cubas, P.; Pazos, F. Breaking-Cas—interactive design of guide RNAs for CRISPR-Cas experiments for ENSEMBL genomes. *Nucleic Acids Res.* **2016**, *44*, W267–W271.
14. Vaughan, A.; Alvarez-Reyes, M.; Bridger, J.M.; Broers, J.L.; Ramaekers, F.C.; Wehnert, M.; Morris, G.E.; Whitfield WGF, W.W.; Hutchison, C.J. Both emerin and lamin C depend on lamin A for localization at the nuclear envelope. *J. Cell Sci.* **2001**, *114*, 2577–90.
15. Sullivan, T.; Escalante-Alcalde, D.; Bhatt, H.; Anver, M.; Bhat, N.; Nagashima, K.; Stewart, C.L.; Burke, B. Loss of A-type lamin expression compromises nuclear envelope integrity leading to muscular dystrophy. *J. Cell Biol.* **1999**, *147*, 913–20.
16. Muchir, A.; van Engelen, B.G.; Lammens, M.; Mislow, J.M.; McNally, E.; Schwartz, K.; Bonne, G. Nuclear envelope alterations in fibroblasts from LGMD1B patients carrying nonsense Y259X heterozygous or homozygous mutation in lamin A/C gene. *Exp. Cell Res.* **2003**, *291*, 352–62.
17. Hale, C.M.; Shrestha, A.L.; Khatau, S.B.; Stewart-Hutchinson, P.J.; Hernandez, L.; Stewart, C.L.; Hodzic, D.; Wirtz, D. Dysfunctional Connections Between the Nucleus and the Actin and Microtubule Networks in Laminopathic Models. *Biophys. J.* **2008**, *95*, 5462–5475.
18. Favreau, C.; Higuet, D.; Courvalin, J.-C.; Buendia, B. Expression of a Mutant Lamin A That Causes Emery-Dreifuss Muscular Dystrophy Inhibits In Vitro Differentiation of C2C12 Myoblasts. *Mol. Cell. Biol.* **2004**, *24*, 1481–1492.
19. Markiewicz, E.; Ledran, M.; Hutchison, C.J. Remodelling of the nuclear lamina and nucleoskeleton is required for skeletal muscle differentiation in vitro. *J. Cell Sci.* **2005**, *118*, 409–420.
20. Meinke, P.; Thuy, D.N.; Wehnert, M.S. The LINC complex and human disease. In Proceedings of the Biochemical Society Transactions; Biochem Soc Trans, **2011**; Vol. 39, pp. 1693–1697.

21. Gerbino, A.; Procino, G.; Svelto, M.; Carmosino, M. Role of Lamin A/C Gene Mutations in the signaling defects leading to cardiomyopathies. *Front. Physiol.* **2018**, *9*.
22. Choi, J.C.; Wu, W.; Muchir, A.; Iwata, S.; Homma, S.; Worman, H.J. Dual specificity phosphatase 4 mediates cardiomyopathy caused by lamin A/C (LMNA) gene mutation. *J. Biol. Chem.* **2012**, *287*, 40513–24.
23. Burla, R.; Torre, M. La; Merigliano, C.; Vernì, F.; Saggio, I. Genomic instability and DNA replication defects in progeroid syndromes. *Nucleus* **2018**, *9*, 368–379.
24. Graziano, S.; Kreienkamp, R.; Coll-Bonfill, N.; Gonzalo, S. Causes and consequences of genomic instability in laminopathies: Replication stress and interferon response. *Nucleus* **2018**, *9*, 289–306.
25. Chen, S.N.; Lombardi, R.; Karmouch, J.; Tsai, J.Y.; Czernuszewicz, G.; Taylor, M.R.G.; Mestroni, L.; Coarfa, C.; Gurha, P.; Marian, A.J. DNA Damage Response/TP53 Pathway Is Activated and Contributes to the Pathogenesis of Dilated Cardiomyopathy Associated with LMNA (Lamin A/C) Mutations. *Circ. Res.* **2019**, *124*, 856–873.
26. Earle, A.J.; Kirby, T.J.; Fedorchak, G.R.; Isermann, P.; Patel, J.; Iruvanti, S.; Moore, S.A.; Bonne, G.; Wallrath, L.L.; Lammerding, J. Mutant lamins cause nuclear envelope rupture and DNA damage in skeletal muscle cells. *Nat. Mater.* **2019**.
27. Ho, C.Y.; Jaalouk, D.E.; Vartiainen, M.K.; Lammerding, J. Lamin A/C and emerin regulate MKL1-SRF activity by modulating actin dynamics. *Nature* **2013**, *497*, 507–11.
28. Bertrand, A.T.; Brull, A.; Azibani, F.; Benarroch, L.; Chikhaoui, K.; Stewart, C.L.; Medalia, O.; Ben Yaou, R.; Bonne, G. Lamin A/C Assembly Defects in LMNA-Congenital Muscular Dystrophy Is Responsible for the Increased Severity of the Disease Compared with Emery-Dreifuss Muscular Dystrophy. *Cells* **2020**, *9*, 844.
29. Steele-Stallard, H.B.; Pinton, L.; Sarcar, S.; Ozdemir, T.; Maffioletti, S.M.; Zammit, P.S.; Tedesco, F.S. Modeling Skeletal Muscle Laminopathies Using Human Induced Pluripotent Stem Cells Carrying Pathogenic LMNA Mutations. *Front. Physiol.* **2018**, *9*, 1332.
30. Chen, C.-Y.; Chi, Y.-H.; Mutalif, R.A.; Starost, M.F.; Myers, T.G.; Anderson, S.A.; Stewart, C.L.; Jeang, K.-T. Accumulation of the inner nuclear envelope protein Sun1 is pathogenic in progeric and dystrophic laminopathies. *Cell* **2012**, *149*, 565–77.
31. Frock, R.L.; Kudlow, B.A.; Evans, A.M.; Jameson, S.A.; Hauschka, S.D.; Kennedy, B.K. Lamin A/C and emerin are critical for skeletal muscle satellite cell differentiation. *Genes Dev.* **2006**, *20*, 486–500.
32. Guelen, L.; Pagie, L.; Brasset, E.; Meuleman, W.; Faza, M.B.; Talhout, W.; Eussen, B.H.; de Klein, A.; Wessels, L.; de Laat, W.; et al. Domain organization of human chromosomes revealed by mapping of nuclear lamina interactions. *Nature* **2008**, *453*, 948–951.
33. Liu, B.; Wang, J.; Chan, K.M.; Tjia, W.M.; Deng, W.; Guan, X.; Huang, J.; Li, K.M.; Chau, P.Y.; Chen, D.J.; et al. Genomic instability in laminopathy-based premature aging. *Nat. Med.* **2005**, *11*, 780–5.
34. Musich, P.R.; Zou, Y. DNA-damage accumulation and replicative arrest in Hutchinson–Gilford progeria syndrome. *Biochem. Soc. Trans.* **2011**, *39*, 1764–1769.
35. Saha, B.; Zitnik, G.; Johnson, S.; Nguyen, Q.; Risques, R.A.; Martin, G.M.; Oshima, J. DNA damage accumulation and TRF2 degradation in atypical Werner syndrome fibroblasts with LMNA mutations. *Front. Genet.* **2013**, *4*, 129.
36. Wolf, C.M.; Wang, L.; Alcalai, R.; Pizard, A.; Burgon, P.G.; Ahmad, F.; Sherwood, M.; Branco, D.M.; Wakimoto, H.; Fishman, G.I.; et al. Lamin A/C haploinsufficiency causes dilated cardiomyopathy and apoptosis-triggered cardiac conduction system disease. *J. Mol. Cell. Cardiol.* **2008**, *44*, 293–303.